

The Fabrication of Freestanding Heterogeneous Copper-Tin Films with Meniscus Brush Plating Electrodeposition

Kimberly Y. Scott^{1,2,*}, Anna Halajko¹ and Glenn G. Amatucci¹

¹Energy Storage Research Group, Department of Materials Science & Engineering, Rutgers University, North Brunswick NJ 08902 USA

²Trainee, Nanotechnology for Clean Energy IGERT

Received: September 17, 2014, Accepted: November 18, 2014, Available online: February 17, 2015

Abstract: A meniscus brush plating electrodeposition technique was utilized in conjunction with a post deposition heat treatment to formulate freestanding copper-tin alloy films for negative electrodes of lithium-ion batteries. The described fabrication technique intertwined the electrode and current collector for improved cell volume utilization and stability. Two designs were examined to establish the best diffusivity to form electrochemically proficient copper-tin alloys. Fabrication was optimized to promote diffusion of copper and tin and to form the desired intermetallic phase of Cu_6Sn_5 . This improved design fabricated films with competitive areal capacities above 1000 mAh/cc and 2.5 mAh/cm² for the complete electrode and current collector structure.

Keywords: Lithium Alloys, Copper-Tin Alloys, Lithium Ion Batteries, Negative Electrodes, Electrodeposition

1. INTRODUCTION

Present work on lithium alloy negative electrodes has focused on silicon and tin due to high lithium uptake compared to current commercial graphite electrodes. Silicon's theoretical capacities of 4199 mAh/g and 9783 mAh/cc easily surpass graphite's capacities of 372 mAh/g and 841 mAh/cc. However, most fabrication and processing modifications are still incapable of absorbing the 320% volumetric expansion for long-term capacity retention [1,2,3,4]. Tin has lower theoretical capacities of 994 mAh/g and 7242 mAh/cc but a lower associated volumetric expansion of 260%, increasing its potential capacity retention with structure manipulation. In contrast to silicon, tin is much more ductile and has better electronic and ionic conductivity [1]. In addition, its capacities both specific and especially volumetric are still much improved versus that of graphite.

Another beneficial aspect is tin's ability to form intermetallic compounds with copper. In a multiphase composite, copper acts as the inactive matrix providing better distribution of large stresses from lithiation and additional networked conductivity when induced stresses cause fracturing of the cycled film [2]. This lithiation of suspended tin within a composite is similar to the role of

SnO forming the irreversible phase of Li_2O , but the copper-tin alloys can be reformed upon delithiation [6,7,8,9,10]. Cu_6Sn_5 , for example, can be fully lithiated in a two-step process with the displacement of copper. The intermediate phase formed with partial Cu displacement is Li_2CuSn . Further lithiation of Li_2CuSn forms $\text{Li}_{22}\text{Sn}_5$ and Cu. Upon delithiation, the Cu_6Sn_5 phase reforms back through the intermediate Li_2CuSn phase [9,10,]. This reaction process helps to alleviate the localized stress induced by volume expansion while providing supportive matrix networking from the copper. Copper is an advantageous host material as its mechanical and electrical properties are well known, and it is currently used as the current collector for commercial negative electrodes.

Several groups have researched the lithiation of Cu_6Sn_5 because of its improved cycling retention over pure tin. Some of their electrochemical findings are summarized in Table 1. Included for comparison is our research on freestanding Cu-Sn films, which will be detailed throughout this paper at a later time. Fabrication techniques utilized include the introduction of graphite to the composite copper-tin system, the utilization of porous structures, and the employment of electrodeposition to produce structured electrodes with improvements in morphology and conductivity [7,9,]. The other groups' results have shown individual improvements for the required electrochemical prerequisites for contesting the current commercial negative electrode. However more developments are

*To whom correspondence should be addressed: Email: kscotty17@gmail.com
Phone: 856-873-1843, Fax: 732-932-6855

essential for creating a complete electrode with increased areal capacities and retention (as seen with our Cu-Sn composite electrode film results in Table 1) since realistic areal capacities above 2 mAh/cm² are required for viable commercial electrode candidates. Such requirements lead to a much higher challenge level for alloys, especially for those fabricated in contiguous structures as stress will impact the thicker, higher capacity electrodes in a much more negative way.

In the following paper, a novel electrodeposition process is developed to fabricate heterogeneous complex copper-tin freestanding films to be used as negative electrodes in lithium ion cells. Electrodeposition is a beneficial process for addressing the issues impeding lithium alloys due to its ability to electrochemically form bonds between film layers utilizing a low cost atmospheric temperature and pressure deposition process. Our optimized technique maximizes the amount of tin available for lithiation (high areal and volumetric capacities) while maintaining capacity retention through a complex architectural system of copper-tin alloys. This fabrication process of Cu-Sn alloys leads to an electrode that fulfills more requirements for a commercial negative electrode, pushing lithium alloys closer to feasibility for these applications.

2. EXPERIMENTAL

2.1. Materials Fabrication

A modified brush plating technique was utilized for the fabrication of electrodeposited Cu-Sn films. The working area was confined to a solution meniscus separating the working and counter electrodes of the deposition process, while a mechanical “pulse” was established with movement of both electrodes during plating by creating a variable residence time. Figure 1 details the simultaneous movement of the counter electrode in the ‘y’ direction and the working electrode in the ‘x’ direction.

A heterogeneous electrode film comprising copper and tin metal was electrodeposited to fabricate removable, freestanding films. The metal films were plated systematically, with the copper film plated first on a titanium substrate, followed subsequently by the tin film. Both films were produced using solutions from SIFCO Applied Surface Concepts: Copper Acid Code 2050/5250 and Tin Code 2093. The copper layer was generated using a constant current between 6.5-8.0 mA/cm². The tin layer was constructed by a constant current between 500-700 μA/cm². Following deposition, the bilayer film was removed from the titanium substrate and thermal annealed to create a freestanding composite film of Cu-Sn intermetallic phases. The triple stacked films included cutting and stacking the bilayer film for the thermal anneal process and will be discussed further at a later time. Heat treatments were conducted in a tube furnace under flowing Argon at 225°C for 4h unless specified otherwise.

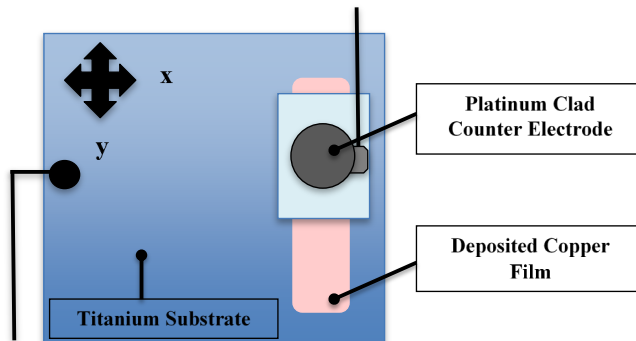


Figure 1. Schematic of the meniscus brush plating setup with a defined movement axis: titanium substrate (working electrode) moves laterally in the ‘x’ direction; counter electrode experiences back and forth movement in the ‘y’ direction

2.2. Physical Characterization

Individual phase identification comprised of x-ray diffraction (Bruker D8 Advance) using monochromatic Cu K_α with the Bragg-Brentano setup. The bilayer films were analyzed from both the top and bottom surfaces to obtain a more precise investigation of the overall composition that may be distorted due to x-ray penetration limits. The x-ray penetration depth was calculated using Equation 1:

$$\tau = \frac{\sin \alpha}{\mu} \quad (1)$$

where τ is the penetration depth, α is the x-ray angle of incidence, and μ is the linear absorption coefficient.

True density was established by He pycnometry (Micromeritics Accu Pyc II 1340) to determine each film’s copper:tin molar ratio and composite film densities. The composite density after thermal anneal was calculated based on the film’s total weight and measured volume by He pycnometry. In addition, electrodeposited individual films of pure copper and tin were analyzed to establish a baseline for densities of each metal. These values were compared to the theoretical values for the pure and intermetallic phases to evaluate our joint deposition and anneal process.

Film morphology and elemental distribution was determined with the Zeiss field emission scanning electron microscopy (FESEM) to analyze the diffusivity of the pure electrodeposited metal films. All samples were cross-sectional ion polished at 5kV for 5h under flowing Argon. The triple stacked bilayer films were supplemented with a silver epoxy coating for additional support

Table 1. Comparison of the electrochemical properties of several composite copper-tin films from Cu-Sn alloy research including our freestanding triple stacked film. Data compiled from references [7,9,12]

Film Description	Lithiated mAh/g (5 th Cycle)	Lithiated mAh/ cm ² (5 th Cycle)	Lithiated mAh/cc (5 th Cycle)	1 st Cycle Irreversible Loss
Codeposition Cu-Sn Films ¹²	390	0.83	3116	10%
Sn ₂₇ Cu ₃₃ C ₄₀ (Milled Cu ₆ Sn ₅ +C) ⁷	170	0.41	1360	29%
Sn ₂₇ Cu ₃₃ C ₄₀ (Sputtered Cu ₆ Sn ₅ +C) ⁷	440	2.17	578	21%
Microporous Cu ₆ Sn ₅ -Sn Foam ⁹	500	1.08	287	13%
Microporous Cu ₆ Sn ₅ -Sn Foam ⁹	670	0.06	705	43%
Triple Stacked Cu-Sn Film 7.5μm Tin Layers	273	3.42	1140	21%

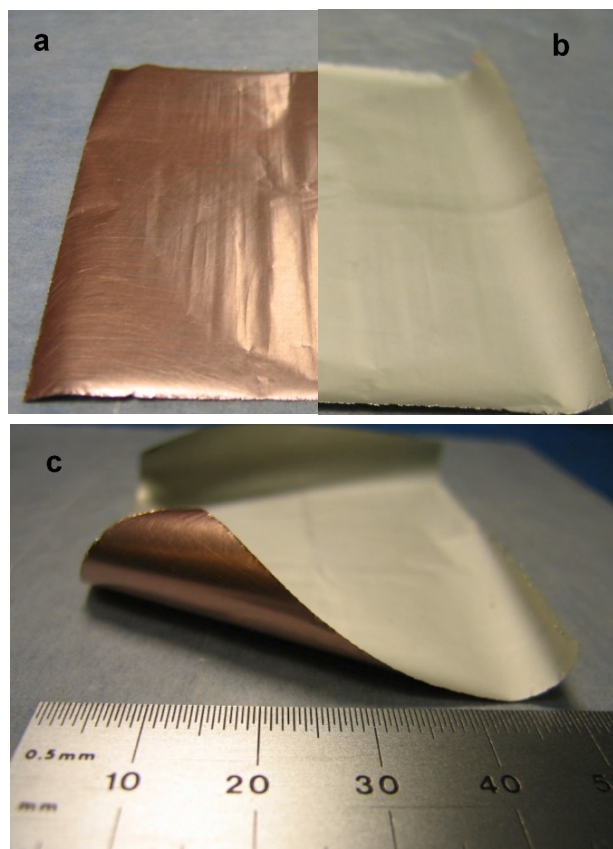


Figure 2. Freestanding electrodeposited Cu-Sn film: a) Bottom of film showing copper layer; b) Top view showing tin layer; c) Curled film shows freestanding capabilities

during polishing. Energy dispersive x-ray spectroscopy (EDS) spectra and maps of the cross-sectional films revealed the elemental mixture of the pure deposited layers after thermal anneal and determined the composite molar ratio for comparison with results obtained by He pycnometry.

2.3. Electrochemical Characterization

Electrochemical analysis of the copper-tin films was accomplished using 316 stainless steel coin cells (Hohsen Corp.) with 1M LiPF₆ Ethylene Carbonate: Dimethyl Carbonate (EC:DMC) 50vol.:%:50vol.% electrolyte (BASF). Half-cells were fabricated with 1/2" diameter electrode film disks versus lithium metal and cycled utilizing a battery cyler (Arbin) under galvanostatic conditions. Two cycling protocols of varying cutoff voltages were utilized with an initial 1.5 cycles at 15 mA/h/g and all further cycling at 30 mA/h/g. The voltage ranges for protocol 1 were 0.01-2V and 0.01-1.3V for protocol 2.

Additional electrochemical evaluation was conducted in lithium ion cells for comparison using MCMB 25-28 graphite anodes. Aluminum coin cells (Hoshen Corp.) with 1M LiPF₆ EC:DMC 50vol.:%:50vol.% electrolyte (BASF) were utilized with 1/2" diameter disks of LiCoO₂ 3 mA/h/cm² cathodes versus the deposited copper-tin film anodes. The full cells were cycled from 2.5-4.15 V for 1000 cycles at 15 mA/g (LiCoO₂).

3. RESULTS & DISCUSSION

3.1. Thin Bilayer Copper-Tin Films: 5.68 micron Tin Layer

The initial electrodeposited films of 3 μm of copper followed by 5.68 μm of tin metal, resulted in a 1.33:1 molar ratio of deposited copper:tin based on thickness of the layers and the pycnometry of the pure layers. Figure 2 shows an image of the freestanding deposited bimetallic film. XRD confirmed the single-phase depositions of Cu (Fm-3m) and Sn (I41/amd) by individual top surface analysis.

Heat treatment at 225°C 4h yielded the composite density of 8.077 g/cc (targeted intermetallic phase Cu₆Sn₅ has a theoretical density of 7.989 g/cc) and the intermetallic phase distribution described in Table 2 from XRD analysis. Top and bottom XRD analysis were utilized to compensate for the limitations of the x-ray penetration depth (8.5 μm) because the total film thickness was 18 μm. As expected from visual observations, the bottom surface x-ray confirms pure copper present within the film along with the formation of alloy phases. Although Cu₆Sn₅ (C2/c) and CuSn (P6[3]/mmc) are respectively monoclinic and hexagonal, these structures are similar leading to sets of convoluted Bragg reflections difficult to distinguish from each other as seen in Figure 3 of the top surface XRD analysis. These phases will therefore be referred as the single phase Cu₆Sn₅/CuSn. Due to these convolutions and determined preferential orientation of the phases, further structural examination with Rietveld analysis has not been successfully executed because of the alloy complexity. Variations in the intermetallic and pure phases for the two directions of XRD analysis reveal the diffusion of the two metals is not uniform throughout the composite. With about 96% of the composite film covered by the two directions of x-ray penetration, the overall distribution suggests that the molar ratio of 1.33:1 is more favorable for producing Cu₃Sn as the dominant intermetallic phase and Cu₆Sn₅/CuSn as the secondary phase.

Figure 4 shows the initial voltage profile of the annealed thin single bilayer 1.33:1 copper:tin film. As is well known, the lithiation of a Cu-Sn alloy film contrasts with the lithiation of pure Sn as discussed by Wang et al and Kitada et al [10,13]. Pure Sn undergoes a direct electrochemical reaction to form the Li_xSn alloy phases resulting in large volumetric expansion, cracking, and excessive SEI development resulting in poor cycling stability. The Cu-Sn alloys require the extrusion of copper for lithiation, providing added stress distribution and enhancement in electronic conductivity, which can improve the cycling stability of the active material. Kitada describes the lithiation of the individual phases Cu₃Sn and Cu₆Sn₅ [13]. Cu₆Sn₅ is considered the more active phase for lithiation due to increased Sn content and has the best cycling stability due to the intermediate phase formation (Li₂CuSn) bridging the volumetric changes for a more gradual stress distribution. Cu₃Sn is less active at room temperature with less Sn content and does not undergo this intermediate step and ultimately has poorer cycling

Table 2. XRD of a 225°C 4h annealed single bilayer 5.68 μm Cu-Sn film

Analysis Direction	Cu	Sn	Cu ₃ Sn	Cu ₆ Sn ₅ /CuSn
Top of Film	0%	10%	67%	22%
Bottom of Film	29%	29%	34%	8%

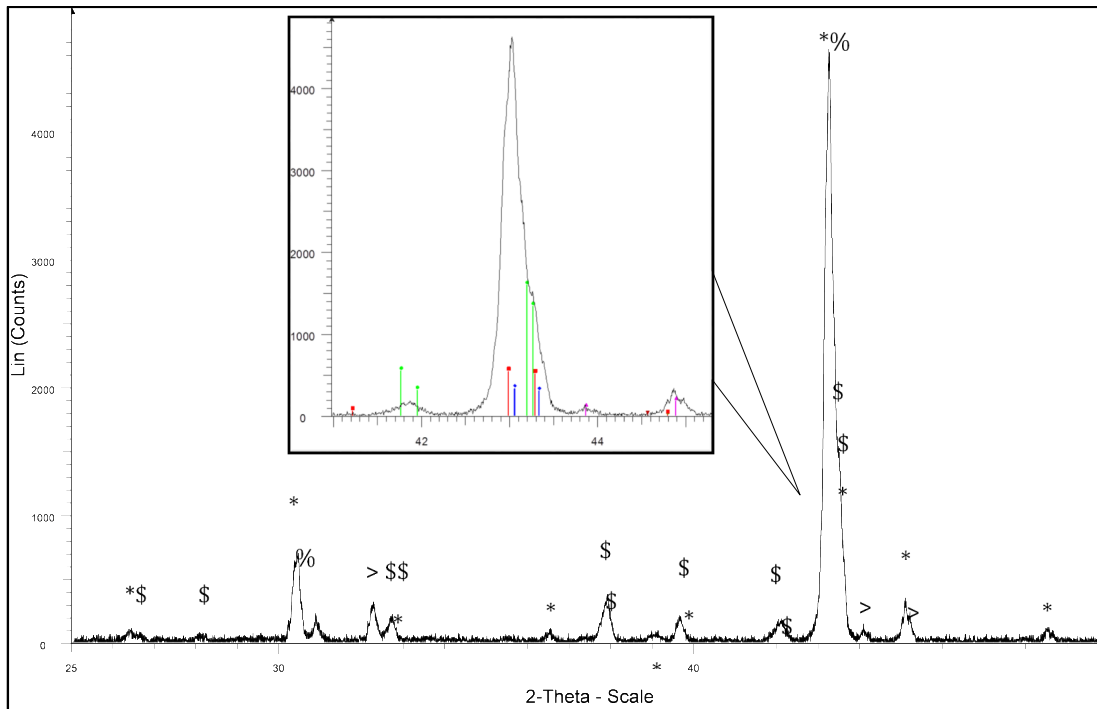


Figure 3. XRD top surface analysis for the 1.33:1 molar ratio film with phases identified as: Cu_6Sn_5 (*), $\text{Cu}_{3.02}\text{Sn}_{0.98}$ (\$), CuSn (%), Sn (>). The inset magnified XRD analysis identifies the peaks for Cu_6Sn_5 (■ red), $\text{Cu}_{3.02}\text{Sn}_{0.98}$ (● green), CuSn (◆ blue), Sn (▲ magenta).

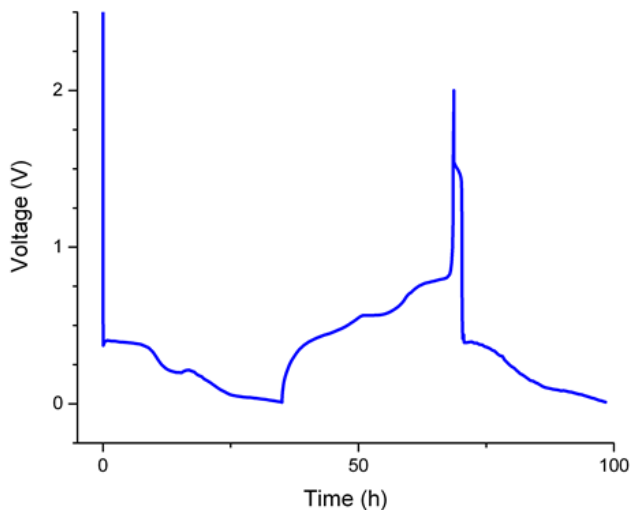


Figure 4. Voltage vs. time for the initial 1.5 cycles of the single bilayer 5.68 μm Cu-Sn film

stability than Cu_6Sn_5 . A mixture of the phases should provide additional stress buffering through the different reactions occurring with lithiation but the total capacity would be dependent on the dominant Cu-Sn phase component. Copper extrusion modifies the potential that the lithium alloys begin to form within the electrode and reduces the dramatic stresses to the Sn active material with the copper buffer. This is confirmed by the onset potential for lithiation of our electrodeposited Cu-Sn composite at 0.38V, which is lower

then the described lithiation curve for pure tin by Huggins [14]. Lowering the onset reaction to form the lithium alloys suggests that little oxide contamination exists and there is minimal initial reaction with the electrolyte to form SEI. The latter usually occurs in the voltage range of 0.5-1.2V. The joint deposited/thermal anneal process developed confirmed we successfully allowed for tin lithiation devoid of large irreversible losses associated to SEI formation. Based on the tin weight in the 1.33:1 bilayer film and calculated density from pycnometry, the film experimental volumetric capacity achieved consisted of 5316 mAh/cc, equivalent to 74% of the theoretical 7202 mAh/cc capacity. It was determined that residual tin was inaccessible for lithiation established by the architectural structuring within the film. Moving forward, a slightly lower density composite film that can provide easier lithium access via fast solid state Li^+ diffusion will be strived for. Analysis of the composite electrode from the composition aspect helps to determine that the Cu_3Sn dominant film has poor cycling capabilities. Since past research suggests that the Cu_6Sn_5 phase is favorable for high capacity achievement and electrochemical stability, the film Cu:Sn molar ratio was adjusted to endeavor preferentially forming $\text{Cu}_6\text{Sn}_5/\text{CuSn}$ [9,10,13,14].

3.2. Thick Bilayer Copper-Tin Films: 17 micron & 8 micron Tin Layers

Thicker bimetallic films were fabricated to investigate if the deposited film ratios or diffusion limitations were the driving factor in low phase transformation to Cu_6Sn_5 (the high capacity Cu-Sn alloy phase). Two molar ratios were investigated in this thicker bimetallic film format: larger copper excess (2.57:1 Cu:Sn) as well as with tin excess (1:1.22 Cu:Sn). In both sets of films, the Cu

thickness remained constant at 10 μm while the Sn varied from 8 to 17 μm respectively.

The tin excess bilayer film, 10 μm of copper metal and 17 μm of tin metal, had a molar ratio of 1:1.22. Due to the large increase in tin content and film thickness, several anneal temperatures and times were investigated as shown in Table 3. Sufficient diffusion to develop intermetallic phases was not achieved until 275°C 4h, resulting in the formation of $\text{Cu}_6\text{Sn}_5/\text{CuSn}$ and Cu_3Sn and the addition of a small amount of SnO. Table 3 only examines the top surface XRD analysis for these films due to the copper layer thickness exceeding x-ray penetration depth, resulting in bottom surface analysis of nearly 100% copper phase for each of the films. The poor phase development in these films led to poor electrochemical performance as described in Table 4. The non-annealed, 150°C 8h, and 200°C 4h annealed films experienced detrimental initial cycling with approximately 100% irreversible loss and low resultant volumetric and areal capacities by the 5th cycle. The thick bilayer film annealed 275°C 4h had low irreversible loss (8%) and decent areal capacity of 2.13 mAh/cm². Further examination of the capacity retention in Figure 5 showed that both the phase development assessed and undetected by the limitations of the XRD penetration depth were not sufficient to avoid early decrepitation and additional cycling irreversible loss. This helped to conclude that the tin excess bilayer film was not capable of achieving the set goals of this project.

The copper excess thick bilayer film was fabricated from 10 μm copper and 8 μm tin (molar ratio of 2.57:1). Different anneal temperatures were analyzed for their phase compositional effects in Table 5, while Table 6 examined the cycling properties and irreversible loss for these films. Similar to the tin excess film (1:1.22 molar ratio), the copper thickness (10 μm) for the 2.57:1 molar ratio film impeded bottom XRD analysis from showing phase formation other than the pure copper phase and has been omitted from the described XRD results (Table 5). The 225°C 8h film dominated

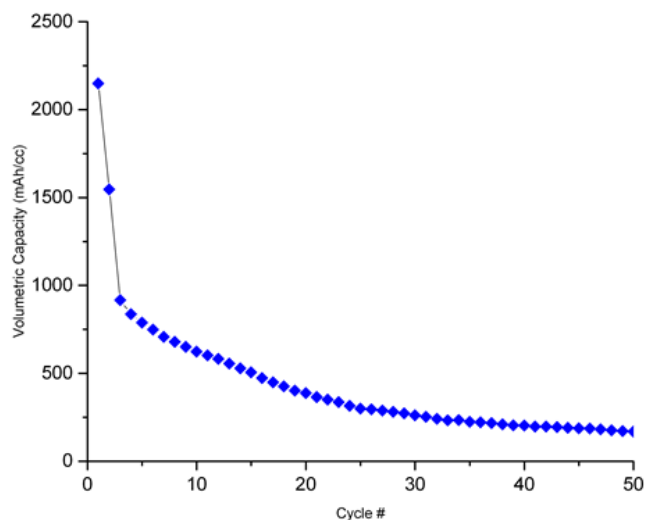


Figure 5. Electrochemical analysis of the annealed 275°C 4h thick bilayer (1:1.22 molar ratio) film showing the poor lithiated (\blacklozenge) volumetric capacity retention over 50 cycles despite low initial irreversible loss

by the Cu_3Sn phase (41%) and high pure tin content (26%) had good areal capacity following the initial irreversible loss, but further analysis revealed poor retention beyond the 5th cycle. The latter was attributed to the effects of lithiating pure tin. The 275°C 4h film had the highest percentage $\text{Cu}_6\text{Sn}_5/\text{CuSn}$ (61%) and low pure tin (6%) but a larger amount of SnO (23%), which can account for the large initial irreversible loss (48%). The volumetric (992 mAh/cc) and areal (1.89 mAh/cm²) capacities at the 5th cycle were higher for this film but did not maintain a stable capacity retention in the long term. The 275°C 24h film, Cu_3Sn phase dominant

Table 3. XRD analysis (top) for the annealed thick single bilayer Cu-Sn films (10 μm :17 μm)

Film Anneal	SnO	Sn	Cu_3Sn	$\text{Cu}_6\text{Sn}_5/\text{CuSn}$
Non-Ann	0%	100%	0%	0%
150°C 8h	0%	100%	0%	0%
200°C 4h	0%	100%	0%	0%
275°C 4h	14%	1%	28%	57%

Table 5. XRD analysis for the annealed thick single bilayer Cu-Sn (10 μm :8 μm) films

Film Annealed	SnO	Sn	Cu_3Sn	$\text{Cu}_6\text{Sn}_5/\text{CuSn}$
225°C 8h	2%	26%	41%	3%
275°C 4h	23%	6%	10%	61%
275°C 24h	7%	6%	58%	29%
325°C 4h	6%	4%	70%	20%

Table 4. Electrochemical analysis of the thick single bilayer Cu-Sn (10 μm :17 μm) films showing the gravimetric, areal, and volumetric lithiated capacities and the initial irreversible loss. The irreversible loss is defined as the difference between the first lithiation and delithiation

Film Anneal	Lithiated mAh/g (5 th Cycle)	Lithiated mAh/cm ² (5 th Cycle)	Lithiated mAh/cc (5 th Cycle)	Irreversible Loss %
Non-Ann	6	0.10	36	100%
150°C 8h	45	0.80	295	99.9%
200°C 4h	0	0	0	100%
275°C 4h	172	2.13	789	8%

Table 6. Electrochemical properties of the thick single bilayer Cu-Sn (10 μm :8 μm) films. The difference in the first lithiation/delithiation is defined as the irreversible loss

Film Anneal	Lithiated mAh/g (5 th Cycle)	Lithiated mAh/cm ² (5 th Cycle)	Lithiated mAh/cc (5 th Cycle)	Irreversible Loss %
225°C 8h	126	1.39	579	14%
275°C 4h	165	1.89	992	48%
275°C 24h	173	2.55	1160	29%
325°C 4h	25	0.24	143	23%

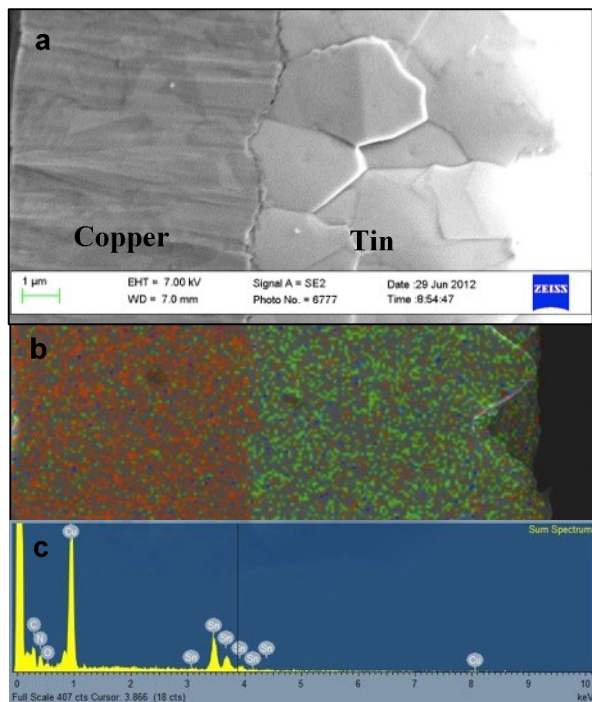


Figure 6. FESEM & EDS analysis of non-annealed thick single bilayer film (10 μm : 8 μm); a) Secondary electron image of tin plated on plated copper film; b) EDS elemental mapping of two different metal films; c) Wide field EDS spectra for identified metal films

(58%), had the highest volumetric and areal capacities with mediocre initial irreversible loss leading to poor longer term capacity retention as expected. Finally, the 325 $^{\circ}\text{C}$ 4h heat-treated film produced the highest amount of Cu_3Sn (70%) with only 20% $\text{Cu}_6\text{Sn}_5/\text{CuSn}$, which lead to low accessible tin for lithiation and much lower capacities also as expected. Overall the intended phase distribution (Cu_6Sn_5 dominant film with low pure Sn, SnO , and Cu_3Sn phases) from the 2.57:1 molar ratio was not achieved and further characterization was needed to understand the phase development within these films.

Microscopy analysis conducted on the cross section of the thick bilayer films (10 micron:8 micron) investigated the elemental distribution, morphology, and structural network. Figure 6 and Figure 7 compare the transformation of the film from the non-annealed state to the thermal anneal transformation at 225 $^{\circ}\text{C}$ 8h. This comparison and direct identification of the copper and tin within each film provides evidence that the copper from the bottom of the film, even with the decrease of the tin, is still restricted from full diffusion to promote the $\text{Cu}_6\text{Sn}_5/\text{CuSn}$ phase. Other annealed 10 micron: 8 micron films similarly confirmed the existence of pure tin and copper at their respective top and bottom surfaces of the film. This concludes that the reduction of the tin layer from the 1:1.22 molar ratio film to the 2.57:1 film was still unable to achieve full diffusion to form the desired intermetallic phases. Therefore, to maximize phase transformations with $\text{Cu}_6\text{Sn}_5/\text{CuSn}$ as the dominant phase and limit the undesired components of pure Sn and Cu_3Sn , an alternative electrodeposited film approach was needed for increased

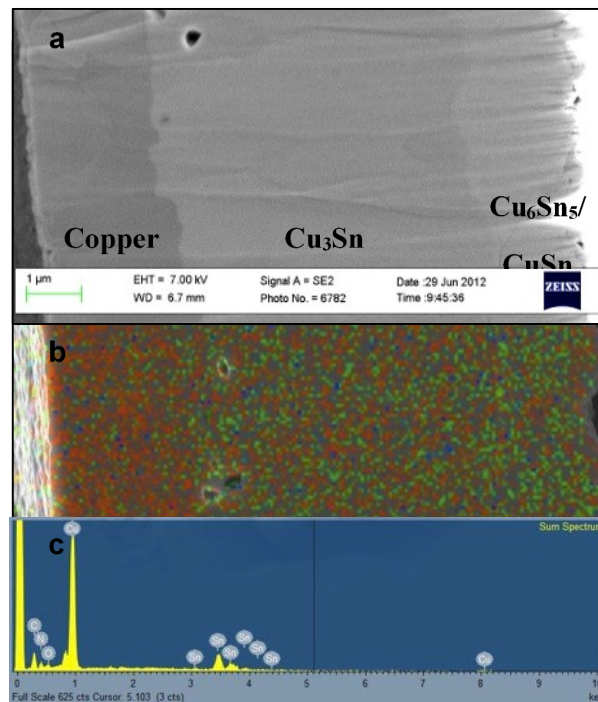


Figure 7. FESEM (a) EDS (b and c) of 225 $^{\circ}\text{C}$ 8h thick single bilayer film (10 μm : 8 μm) annealed for 225 $^{\circ}\text{C}$ 8h

diffusion capabilities without the sacrifice of electrochemical properties.

3.3. Triple Stack Thin Copper-Tin Films

3.3.1 Structure Analysis of Triple Stacked Bilayer Films

Three thinner bimetallic Cu-Sn films were stacked and annealed in order to induce more facile diffusion of the Cu-Sn species for the formation of the desired $\text{Cu}_6\text{Sn}_5/\text{CuSn}$ intermetallics and high areal capacities. Aside from potential as a viable current collector, the copper within the film provided support as a buffering matrix layer for tin lithiation, resulting in better distributed stresses and prolonged cycling. Multi-layered alternating electrodeposition of copper and tin was considered briefly but impeded by the production of electroless plated copper following deposited tin metal. Electroless deposition occurs because of the higher redox potential of the Cu^+ relative to Sn^{2+} and proceeds uncontrollably during brush plating.

3.3.2. 225 $^{\circ}\text{C}$ 4h Thermal Anneal of Triple Stacked Bilayer Film

The effect of increasing tin content was examined by the fabrication of a 3 μm Cu film with increasing thicknesses of Sn: 5.68 μm , 6.5 μm and 7.5 μm . Based on weight, these three films represent a molar ratio of 1.33:1, 1.17:1, and 1:1.04 of Cu:Sn for the 5.68 μm , 6.5 μm and 7.5 μm , respectively. The central portion of each completed Cu-Sn bilayer film was extracted, divided, and stacked accordingly. Each film was pressed between stainless steel plates and annealed at 225 $^{\circ}\text{C}$ under Argon flow for 4h. The final measured densities for the 5.68 μm , 6.5 μm and 7.5 μm stacked films were

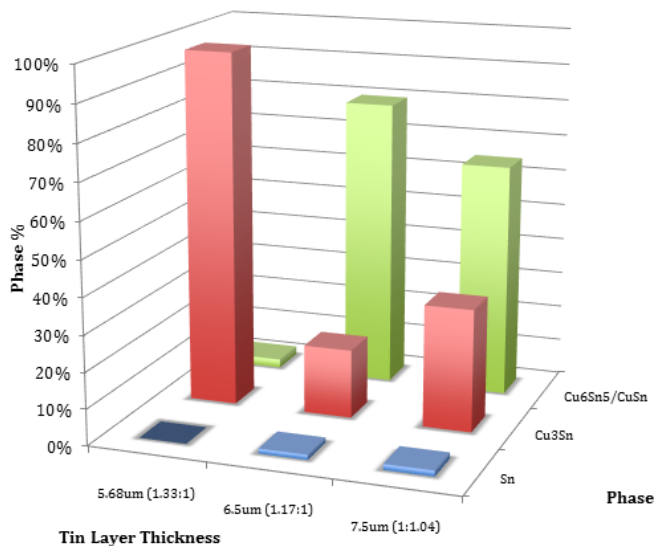


Figure 8. Comparison of the XRD phase for the triple stacked bilayer Cu-Sn films annealed at 225°C 4h as a function of Sn content (top surface analysis)

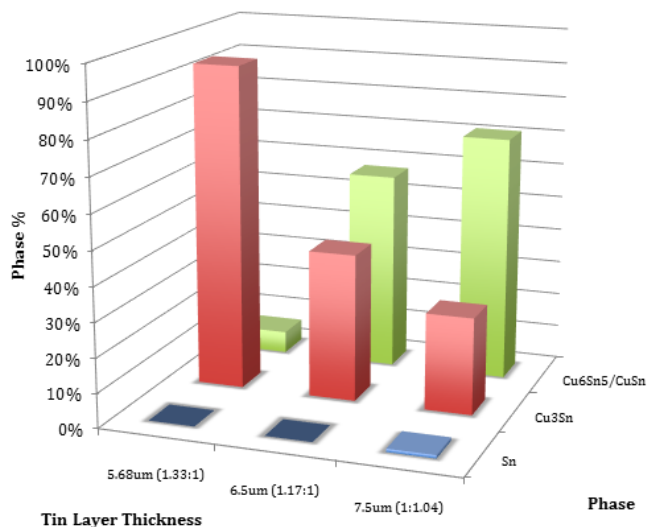


Figure 9. Comparison of phases as determined by XRD for the triple stacked bilayer Cu-Sn films annealed at 225°C 4h cycled with 1.3V cutoff (top surface analysis)

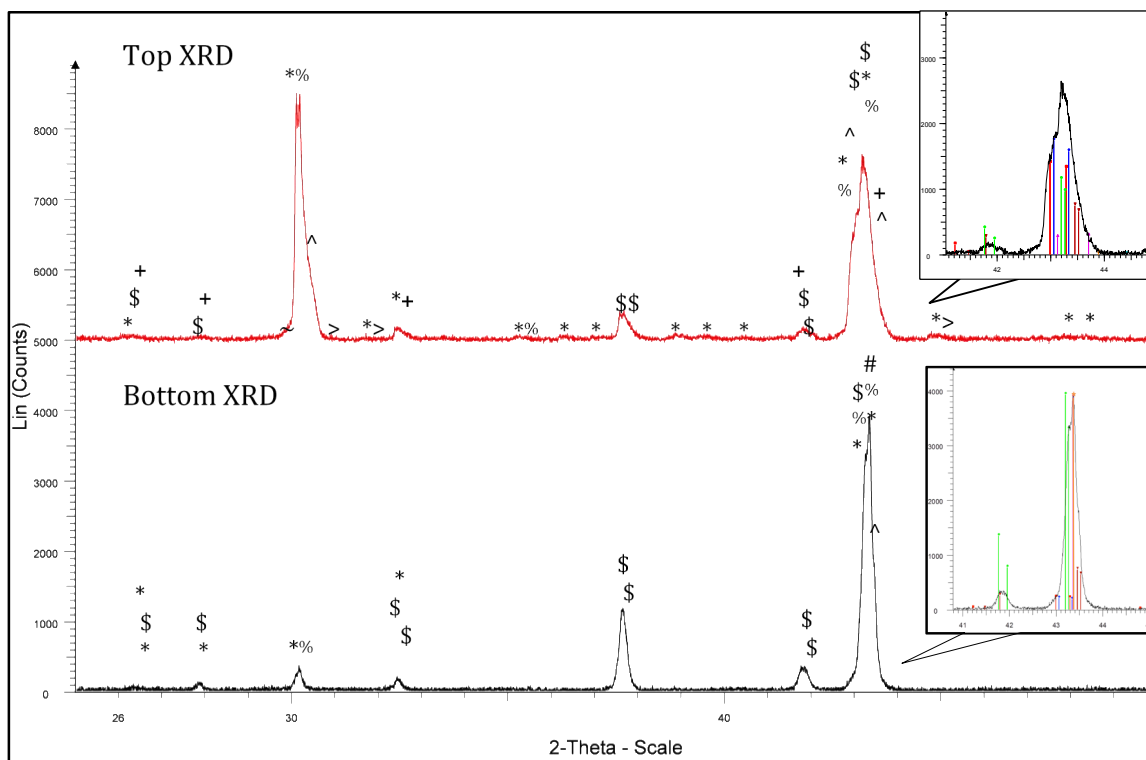


Figure 10. The phases of the 6.5 μm triple stacked film (top and bottom surface analysis) identified as: Cu_6Sn_5 (*), $\text{Cu}_6\text{Sn}_5'$ (^), $\text{Cu}_{3.02}\text{Sn}_{0.98}$ (\$), Cu_3Sn (+), CuSn (%), Sn (>), SnO (~), Cu (#). The magnified inset XRD analysis identifies the peaks for Cu_6Sn_5 (red), $\text{Cu}_6\text{Sn}_5'$ (magenta), $\text{Cu}_{3.02}\text{Sn}_{0.98}$ (green), Cu_3Sn (maroon), CuSn (blue), and Cu (orange)

8.435 g/cc, 8.231 g/cc, and 8.14 g/cc, respectively. The composite film thicknesses were 15-20 μm (1.33:1), 20-25 μm (1.17:1), and 30 μm (1:1.04) for each of the triple stacked films.

XRD phase analysis from the top and bottom surfaces of the

stacked film revealed pure Sn was present in residual amounts on the order of 1-2% as identified for the 1.17:1 and 1:1.04 molar ratio stacked films and non-existent for the 1.33:1 molar ratio as shown in Figures 8-9. Diffusion formed the intermetallic phases of Cu_3Sn

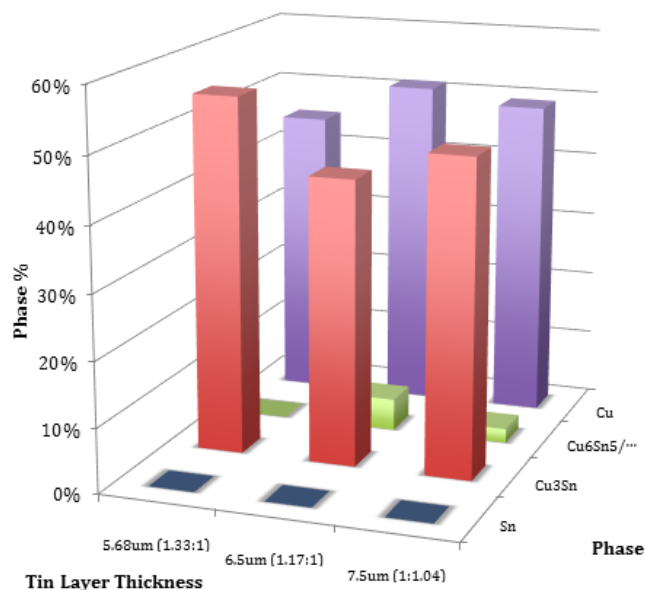


Figure 11. XRD phase analysis for the triple stacked Cu-Sn films (bottom surface analysis)

and Cu₆Sn₅/CuSn. The 1:1.04 molar ratio films were dominated by the Cu₆Sn₅/CuSn phase ranging from 65-71% and contained 28-34% Cu₃Sn. Similarly, the 1.17:1 molar ratio films had lower amounts of Cu₃Sn (19-43%) and dominance of the Cu₆Sn₅/CuSn phase (57-80%). As expected, the 1.33:1 molar ratio films contained 94-98% Cu₃Sn and small amounts of Cu₆Sn₅/CuSn, 2-6%. The alloy complexity is shown in Figure 10 for the 1.17:1 molar ratio stacked film top and bottom investigations. Figure 11 shows the results of the XRD analysis for the bottom surface of the films. XRD of the bottom surface of the stacked films reveals the domination by the pure Cu phase for all three ratios at roughly 50%, followed by the intermetallic phase, Cu₃Sn. In combination with the top surface XRD results, it is concluded that much improved distribution of Cu is achieved from the alternating bimetal design due to the lack of pure tin present following thermal anneal. The additional pure copper only present in the bottom of the triple stacked film provides a built-in current collector for the electrode, which from the commercial standpoint, can be beneficial in maximizing cell design space. The Cu is only present on the bottom of the triple stack as it is the only copper layer not bordered on both sides by a corresponding layer of Sn.

Figure 9 shows a decreasing trend of the Cu₃Sn phase and increase of the Cu₆Sn₅/CuSn phases with the increase of Sn molarity of the triple stacked films. All molar ratios showed the existence of minimal pure tin following the anneal heat treatment. This confirms

the stacking of thinner films successfully combined the pure copper and tin phases to produce the maximum amount of alloy phases for each of the film thicknesses. The theoretical molar ratios for Cu₃Sn, Cu₆Sn₅, and CuSn are 1.63:1, 1:1.56, and 1:1.86, respectively. Their coinciding theoretical densities are 8.348 g/cc, 7.989 g/cc, and 7.922 g/cc, accordingly. When the pycnometer-measured densities of the stacked films were compared to these values and the XRD compositional analysis, the trending increase of the Cu₆Sn₅/CuSn phase with the increase of deposited tin per layer is supported.

The theoretical x-ray penetration depth as a function of molar ratio was calculated to shed insight on the relevance of the XRD data. Table 7 examines the calculated x-ray penetration depth for each film. Based on the depth of penetration, it is confirmed that full phase analysis required both top and bottom directional investigation due to total thickness. However, the x-rays easily penetrated the top bilayer film in each of the stacks showing no signs of pure copper from the first internal layer. Therefore, our XRD data is well representative of the amount of Sn that has converted to the intermetallic phases due to the full diffusion of copper.

3.3.3. Cross Section Analysis

Phase and morphological distribution of each stacked bilayer film was provided by the cross-sectional analysis via FESEM microscopy. Figures 12-14 details the copper and tin distribution throughout the 7.5 µm (1:1.04), 6.5 µm (1.17:1), and 5.68 µm (1.33:1), respectively. The elemental analysis for each of the films confirms the copper layer of the top two bilayers has been completely transformed so the only copper dominant area remaining for the annealed film is a small portion of the underside bottom bilayer. This is consistent with the aforementioned fact that the bottom Cu is not bordered on both sides by Sn to diffuse into. A distinct boundary for each of the intermetallic phases was not observable in comparison to the FESEM and EDS images of the thick single bilayer films seen in Figure 7. Further investigations of the spectra collected during EDS helped determine the overall copper and tin content for each film. The measured molar ratio for each film was 1:1.04, 1:1.17, and 1.86:1 for the 7.5 µm, 6.5 µm, and 5.68 µm, respectively. These values were slightly different from the derived values from the pycnometer analysis of 1:1.04 (7.5 µm), 1.17:1 (6.5 µm), and 1.33:1 (5.68 µm) and the targeted theoretical molar ratio for Cu₆Sn₅, 1:1.56. Differences in the values are attributed to variations within the film from inhomogeneities of the electrodeposition process and phase distribution.

3.3.4. Electrochemical Investigations For Triple Stacked Bilayer Films

The fabricated films were tested for their electrochemical activity utilizing the two described cycling protocols. Protocol 1 examines the cycling stability with a delithiation cutoff of 2V while protocol

Table 7. X-ray penetration depth based on single direction analysis for triple stacked films

Film	Molar Ratio (Cu:Sn)	Calculated X-ray Penetration Depth	Film Thickness	Percent Film by XRD
5.68µm	1.33:1	8.44 µm	15-20 µm	42-56%
6.5µm	1.17:1	7.86 µm	20-25 µm	31-39%
7.5µm	1:1.04	7.27 µm	30 µm	24%

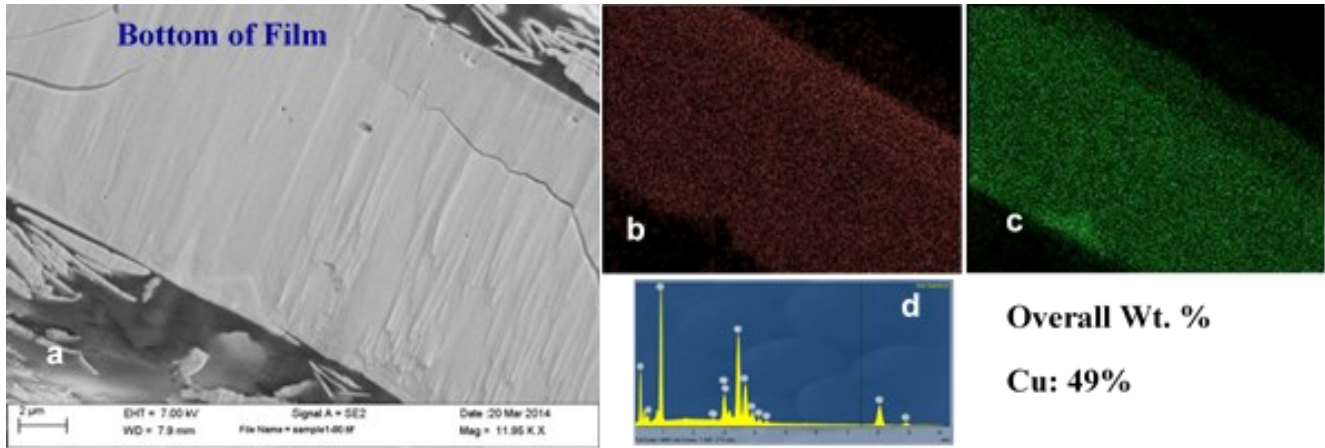


Figure 12. FESEM & EDS images and spectrum for the triple stacked 7.5 μm bilayer film (1:1.04 molarity); a) Secondary electron image detailing cross-sectional view of stacked film; b) EDS elemental analysis of copper content; c) EDS elemental analysis of tin content; d) Spectra results for 7.5 μm triple stacked bilayer film

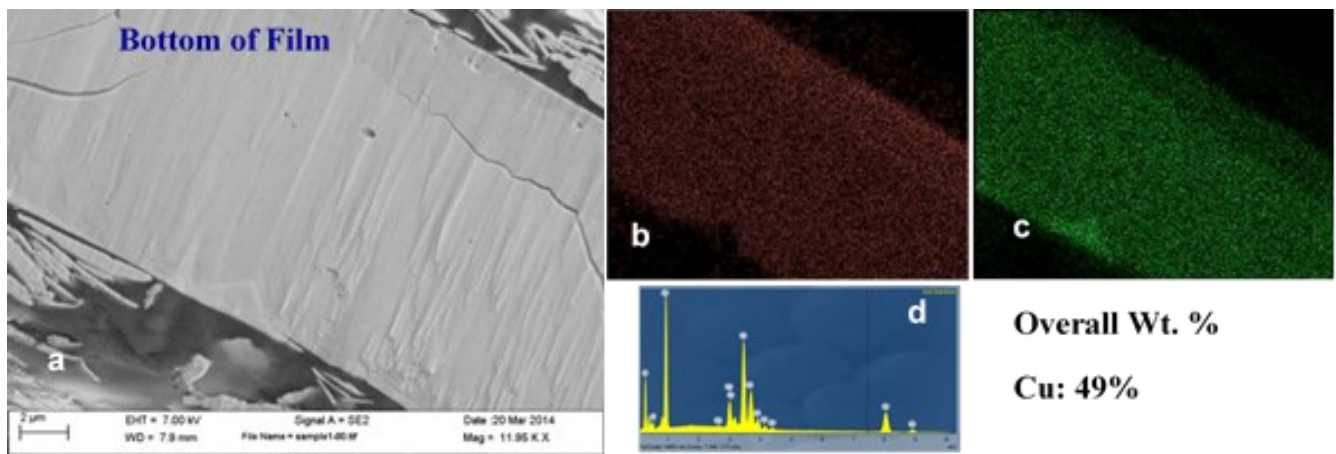


Figure 13. FESEM & EDS images and spectrum for the triple stacked 6.5 μm bilayer film (1.17:1 molarity); a) Secondary electron image detailing cross-sectional view of stacked film; b) EDS of copper content; c) EDS of tin content; d) Spectra results for 6.5 μm triple stacked bilayer film

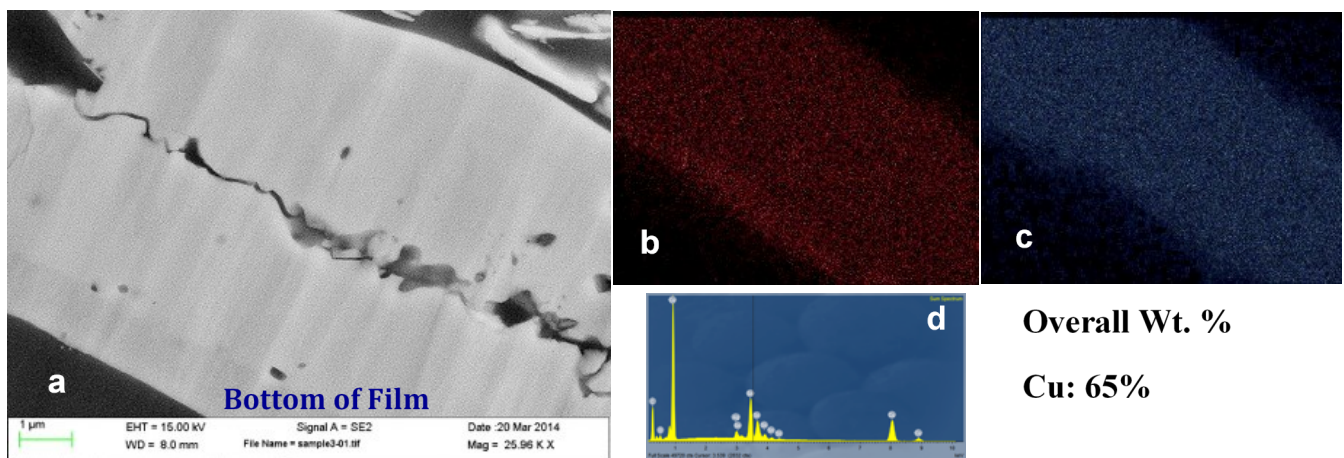


Figure 14. FESEM & EDS images and spectrum for the triple stacked 5.68 μm bilayer film (1.33:1 molarity); a) Secondary electron image detailing cross-sectional view of stacked film; b) EDS of copper content; c) EDS of tin content; d) Spectra results for 5.68 μm triple stacked bilayer film

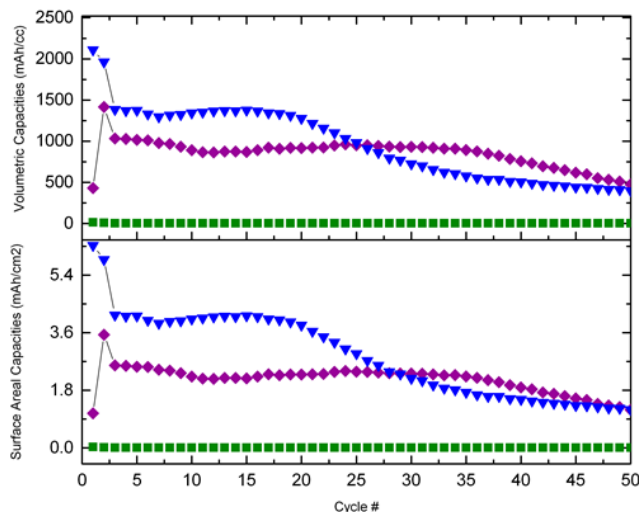


Figure 15. Electrochemical analysis of triple stacked bilayer films for the first 50 cycles utilizing 2V cutoff cycling. ■ - (1.33:1) molar ratio; ◆ - (1.17:1) molar ratio; ▼ - (1:1.04) molar ratio

2 utilizes a lower cutoff of 1.3V. Figures 15 and 16 show the capacity as a function of cycle number for the 2V and 1.3V cutoffs, respectively. Two capacity plots are shown for each protocol based on the volumetric capacity of the entire composite film inclusive of the copper metal and also the electrodes' areal capacities. For the 2V cutoff, the molar ratio of 1.17:1 had the best cycling with good retention to approximately 40 cycles. The volumetric capacity approaches 1400 mAh/cc even at a relatively high areal capacity in the range of 2-3 mAh/cm².

In general, the 1.3V cutoff (Fig. 16) resulted in improved cycling stability for all compositions, consistent with findings by Beattie and Dahn [12]. More specifically, there was a marked improvement in the larger Sn molar ratio film of 1:1.04. The Cu:Sn molarity and electrochemical protocol impact on the electrochemical performance was further analyzed as shown in Table 8 and Table 9. From

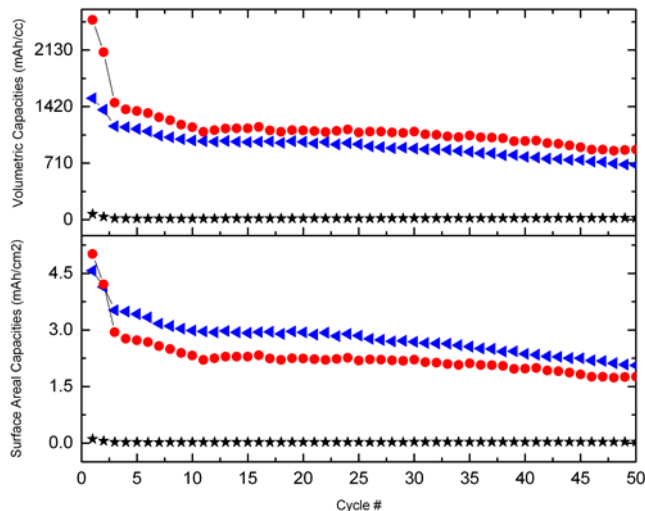


Figure 16. Electrochemical analysis of triple stacked bilayer films first 50 cycles utilizing 1.3V cycling cutoff. ★ - (1.33:1) molar ratio; ● - (1.17:1) molar ratio; ◀ - (1:1.04) molar ratio

this data, it can be concluded that the compositional makeup of the 5.68 μm bilayer stacked film (Cu:Sn molar ratio of 1.33:1) was unfavorable and produced the highest irreversible losses during the first cycle of 67% and 58% for Protocol 1 and 2, respectively. The best composition for producing the lowest irreversible losses (21%) and highest capacities (1375 mAh/cc and very high 4.13 mAh/cm²) was generated from the 7.5 μm triple stacked bilayer films (1:1.04). This composition had lower long-term retention when compared to the 6.5 μm triple stacked film data but was improved by the lower voltage range (cutoff 1.3V) as seen with the comparison of the data. This is partly supported by low onset reactivity described during the early voltage profiles seen in Figure 17. Figure 18 provides the direct comparison of the lithiation and delithiation capacities for the 1:1.04 molar ratio stacked film cycled with this cutoff showing good efficiencies after the first two cycles. It should be noted that

Table 8. Electrochemical findings for the triple stacked Cu-Sn films cycled utilizing the 2V cutoff. Included is the comparison are the initial irreversible loss defined as first lithiation/delithiation difference, gravimetric, areal, and volumetric capacities

Films (Cu:Sn)	Lithiated mAh/g (5 th Cycle)	Lithiated mAh/cm ² (5 th Cycle)	Lithiated mAh/cc (5 th Cycle)	Irreversible Loss %
5.68 μm (1.33:1)	0	0.01	3	67%
6.5 μm (1.17:1)	207	2.54	1015	4%
7.5 μm (1:1.04)	344	4.13	1375	49%

Table 9. Electrochemical results for the triple stacked Cu-Sn films cycled with the 1.3V cycling cutoff. Irreversible loss is defined as difference in first lithiation/delithiation

Films (Cu:Sn)	Lithiated mAh/g (5 th Cycle)	Lithiated mAh/cm ² (5 th Cycle)	Lithiated mAh/cc (5 th Cycle)	Irreversible Loss %
5.68 μm (1.33:1)	2.5	0.02	15	58%
6.5 μm (1.17:1)	229	2.73	1363	40%
7.5 μm (1:1.04)	273	3.42	1140	21%

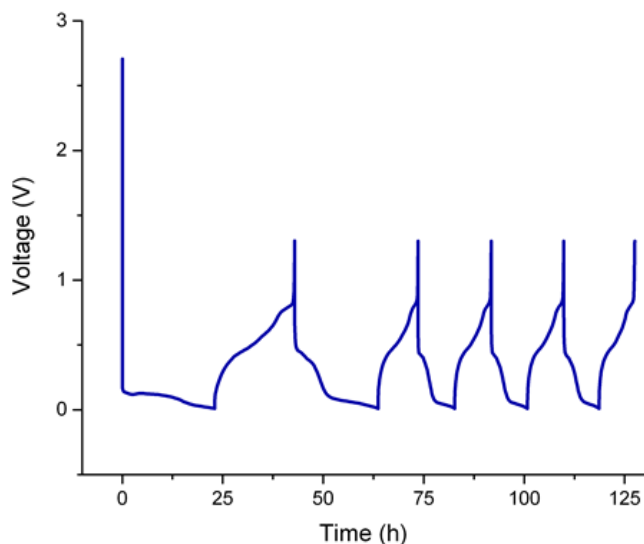


Figure 17. Voltage vs. time profiles for the first 5 cycles of 1:1.04 molar ratio (7.5µm) stacked film with 1.3V cutoff

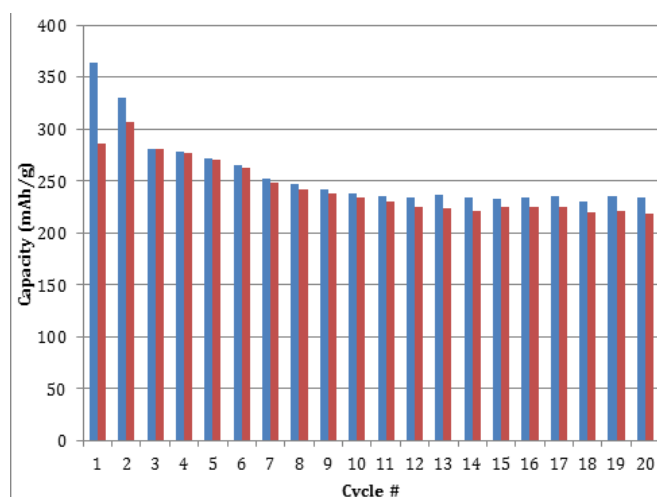


Figure 18. Charge-discharge efficiencies for the 7.5 µm (1:1.04 Molarity) triple stacked film depicted by the comparison of lithiation (■) and delithiation (■) capacities for the 1.3V cycling cutoff

the analysis was carried out using a standard electrolyte composition of LiPF_6 EC:DMC and much improvement in efficiencies can be brought about by the select use of additives. However, this was not the focus of the present communication.

The relationship of film Cu:Sn molarity to electrochemistry for the 6.5 µm (1.17:1) and 7.5 µm (1:1.04) films are slightly unclear with similar capacity retention, volumetric and surface areal capacities. Comparisons of electrochemistry and compositions do not show a direct trend leading to an overall better film, but it should be noted that phase analysis revealed similar distributions. As such, the combined data suggests that the creation of a composition with the dominant phase of $\text{Cu}_6\text{Sn}_5/\text{CuSn}$ and limitations to the pure Sn phase and intermetallic, Cu_3Sn , produces the best results. This is

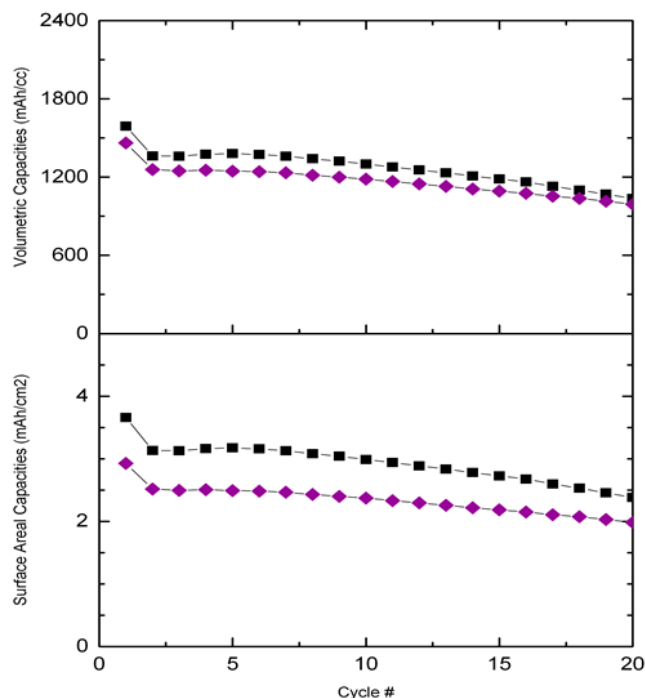


Figure 19. Electrochemical analysis for the first 20 cycles of the triple stacked 6.5 µm (1.17:1 molarity) films in Li-ion cells. ■ - D627; ◆ - D632

confirmed by the results of 6.5 µm (1.17:1 Cu:Sn ratio) for delithiation cutoff of 2V and 7.5µm (1:1.04 Cu:Sn ratio) for delithiation cutoff 1.3V.

4. CU-SN BILAYER FILMS INCORPORATED INTO LI-ION CELLS

The practicality of the electrodeposited triple stacked bilayer films was tested in full lithium ion cells assembled utilizing LiCoO_2 with approximately 3 mAh/cm² versus the Cu-Sn 6.5 µm (1.17:1) stacked films. Due to variability in the deposition process, several cells were produced and their compositional analysis observed. Figure 19 shows the electrochemical plots for the lithiated volumetric and surface areal capacities for the early cycles. The volumetric and areal capacities on the 5th cycle are 1380 mAh/cc and 3.17 mAh/cm² for cell D627 and 1246 mAh/cc and 2.49 mAh/cm² for cell D632. These cells maintained high cycling retention of 91% between cycles 3-13. Obviously, improvement for balanced Li-ion cells are needed, but further optimization needs to be performed with respect to matching ratios, electrode and electrolyte compositions. Overall our electrodeposited films and triple stacked thermal anneal process have thus far proved to produce freestanding negative electrodes for lithium ion cells unlike any other previously mentioned Cu-Sn research. The combined data shows that our technique has the ability to fabricate lithium-alloying electrodes with both high volumetric and surface areal capacities. Although not perfected, this technique may be a viable approach for rapid fabrication of various alloys for Li-ion batteries.

5. CONCLUSIONS

Brush assisted electrodeposition was utilized to manipulate the morphology of copper-tin alloyed films for cycling improvements as negative electrodes in lithium ion batteries. The described films obtained competitive volumetric and surface areal capacities above 1000 mAh/cc and 2.5 mAh/cm², respectively. In addition, this fabrication process subsequently produced a unique freestanding film with a combined current collector and electrode, eliminating the requirement for additives and fillers typically used in commercial production.

6. ACKNOWLEDGEMENTS

The authors acknowledge the financial support of Defense Advanced Research Projects Agency N66001-10-C-2013 and National Science Foundation Grant No. 0903661 "Nanotechnology for Clean Energy IGERT." The authors would also like to thank Barry Vanning, John Gural and Nathalie Pereira for their technical assistance.

REFERENCES

- [1] J. Yang, J.-I. Wang, *Encyclopedia of Electrochemical Power Sources*, 225, (2009).
- [2] W.-J. Zhang, *Journal of Power Sources*, 196, 13 (2011).
- [3] W.-J. Zhang, *Journal of Power Sources*, 196, 877 (2011).
- [4] C. Liang, M. Gao, H. Pan, Y. Liu, M. Yan, *Journal of Alloys and Compounds*, 575, 246 (2013).
- [5] K.D. Kepler, J.T. Vaughey, M.M. Thackeray, *Journal of Power Sources*, 81-82, 383 (1999).
- [6] I.A. Courtney, J.R. Dahn, *Journal of the Electrochemical Society*, 144, A2045 (1997).
- [7] J.S. Thorne, J.R. Dahn, M.N. Obrovac, R.A. Dunlap, *Journal of Power Sources*, 216, 139 (2012).
- [8] D. Larcher, L.Y. Beaulieu, D.D. MacNeil, J.R. Dahn, *Journal of the Electrochemical Society*, 147, A1658 (2000).
- [9] L. Trahey, J.T. Vaughey, H.H. Kung, M.M. Thackeray, *Journal of the Electrochemical Society*, 156, A385 (2009).
- [10] S. Wang, W. Zhao, Y. Wang, X. Liu, L. Li, *Electrochimica Acta*, 109, 46 (2013).
- [11] L. Fransson, E. Nordström, K. Edström, L. Häggström, J.T. Vaughey, M.M. Thackeray, *Journal of the Electrochemical Society*, 149, A736 (2002).
- [12] S.D. Beattie, J.R. Dahn, *Journal of the Electrochemical Society*, 150, A894 (2003).
- [13] A. Kitada, N. Fukuda, T. Ichii, H. Sugimura, K. Murase, *Electrochimica Acta*, 98, 239 (2013).
- [14] R.A. Huggins, *Journal of Power Sources*, 81-82, 13 (1999).